

# Buckling of Aligned Carbon Nanotubes as Stretchable Conductors: A New Manufacturing Strategy

Yong Zhu\* and Feng Xu

Stretchable conductors (interconnects and electrodes) play a key role in the development of stretchable electronics, sensors and energy harvesting/storage devices.<sup>[1]</sup> Carbon nanotubes (CNTs) have high aspect ratio, excellent electric conductivity, high thermal stability and mechanical robustness,<sup>[2]</sup> which make them promising candidates for stretchable conductors. Several methods have been demonstrated for fabrication of CNT-based stretchable conductors, including mixing single-walled CNTs (SWNTs) and ionic liquid in a fluorinated copolymer matrix,<sup>[1f]</sup> depositing SWNT films on polymer films,<sup>[3]</sup> backfilling SWNT aerogels with polymers,<sup>[4]</sup> infiltrating multi-walled CNT (MWNT) forests with polymer binder,<sup>[5]</sup> dispersing MWNTs in polymers by ultrasonication or melt shear mixing,<sup>[6]</sup> and creating out-of-plane buckled MWNT ribbons on polymer films.<sup>[7]</sup>

A successful route to stretchable conductors or device components is to create buckling-induced wavy or coiled architectures out of the otherwise flat building blocks (often inorganic materials). One approach for buckling is as follows: the building blocks are transferred to a prestretched elastomeric substrate; upon release of the prestretch, the building blocks buckle.<sup>[1c,8]</sup> A critical step is to prestretch the substrate, which might present a challenge for large-scale manufacturing process (e.g., roll-to-roll process). In this paper, we present an alternative approach for buckling of the building blocks, which does not involve prestretching the substrate but relies on the interface interaction between the building blocks and the substrate. More specifically, upon stretching the substrate the building blocks slide on the substrate, but upon releasing the substrate the building blocks buckle (instead of sliding back). This stretching/releasing step is after the device manufacturing. Following this new buckling approach, we demonstrated stretchable conductors based on well-aligned CNT ribbons.

The CNT ribbons used in this study were directly drawn from spinable, vertically-grown MWNT forests and then transferred onto PDMS substrates. **Figure 1a** shows a scanning electron microscopy (SEM) image of a CNT ribbon (top view) drawn from the CNT forest. It can be seen that the ribbons are uniformly aligned along the drawing direction. The diameters of the MWNTs in this study typically ranged from 30 to 50 nm. **Figure 1b** shows a fabricated stretchable conductor with a CNT ribbon lying on top of PDMS with good optical transmittance (~40%).

The resistance of a typical CNT/PDMS film (normalized by its initial resistance at zero strain) versus the applied strain is plotted in **Figure 1c**. It can be seen that the resistance first increased almost linearly with increase of the tensile strain up to ~20%. Upon release of the strain, the resistance was unchanged (did not return to its initial value). When stretched back to 20%, the resistance still remained constant. Beyond 20% strain, the resistance increased linearly again with the strain. Similar behaviors were observed for the releasing and stretching processes repeated at the strains of 40%, 60% and 100%. After further stretching/releasing cycles, the resistance was unchanged in the strain range of 0–100%. This electric response as a function of the applied strain was close to the case of CNT embedded in PDMS.<sup>[9]</sup> Naturally the above electric response of the CNT ribbons under strain brought up two questions: 1) what causes the resistance increase during the first stretching and 2) why does the resistance remain nearly constant during the subsequent stretching/releasing?

**Figure 2a** and **b** show optical images of a CNT ribbon on PDMS before and after it was stretched to 80%, respectively. **Figure 2c** shows the CNT ribbon after released to 40% strain, where the CNTs started to buckle and form uniform, periodic wavy structures in the lateral direction. With larger strain release, the wavelength and amplitude of the buckled ribbon became smaller and larger, respectively. **Figure 2d** shows the CNT ribbon after the prestrain is completely removed (zero strain). For clarity, a schematic corresponding to each figure is inserted to show the deformation process of the CNT ribbon. **Figure 2e** shows an SEM image of the CNT ribbon (corresponding to **Figure 2d**). Clearly the initially straight CNTs buckled into wavy structures in the lateral direction. It is interesting to note that most CNTs buckled in bundles rather than individually. The lateral buckling of CNTs is likely related to the electric response shown in **Figure 1c**, but the underlying mechanisms remain elusive (i.e., how exactly are the buckles formed and how does the resistance of buckled CNTs change in response to mechanical strain?)

We designed a model experiment to investigate how the buckles are formed, with four neighboring CNTs on a PDMS substrate (**Figure 3**). The CNTs are artificially colored for clarity (see Supporting Information for the original images before colored). The applied strains in the five panels are 0, 9.2%, 16.1%, 10.4% and 0, respectively. The substrate was stretched/released by a mechanical testing stage under an optical microscope. CNT\_A is partly overlapped with CNT\_B, while CNT\_C has a gap with CNT\_D. Upon stretching, there was no measurable elongation in CNT\_C (the same as the other three CNTs) with the resolution of our optical images. The CNT elongation was measured in the optical images (each image possesses 750 × 480 pixels and a CNT typically spans 200–250 pixels in

Prof. Y. Zhu, F. Xu  
Department of Mechanical and Aerospace  
Engineering, North Carolina State University  
Raleigh, North Carolina 27695-7910, USA  
E-mail: yong\_zhu@ncsu.edu



DOI: 10.1002/adma.201103382

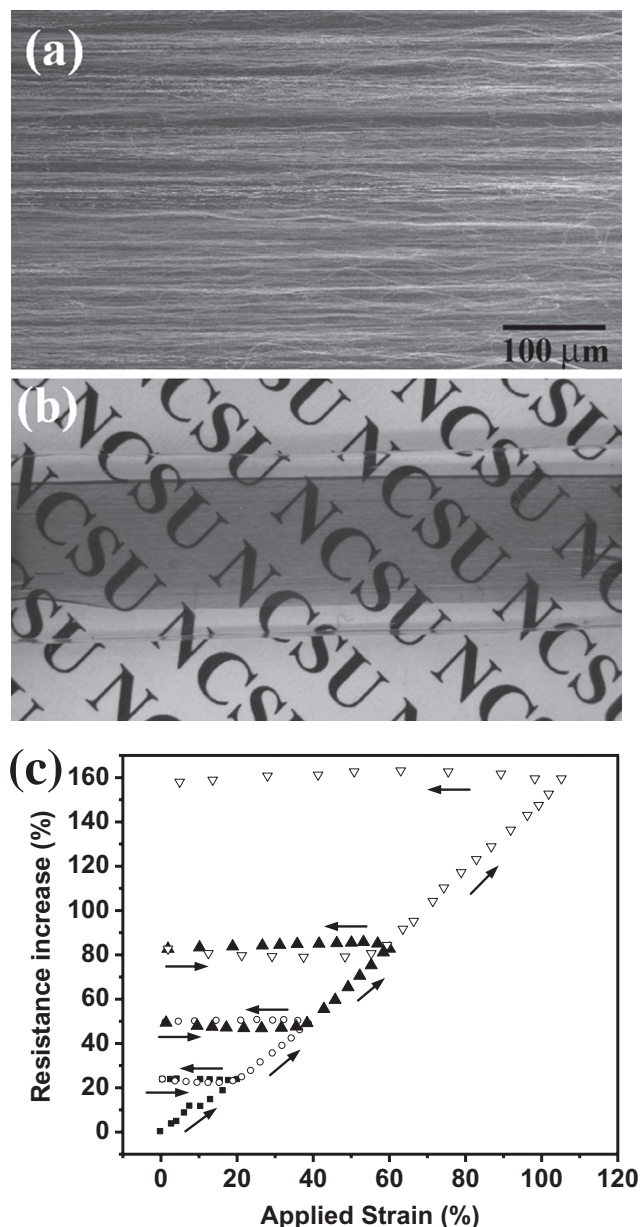


**Figure 1.** (a) Top view SEM image of a CNT ribbon. (b) Optical image of a CNT/PDMS film on top of a printed paper with “NCSU”, showing good optical transmittance. (c) Resistance change of a typical CNT/PDMS film as a function of applied strain. Each symbol represents one loading-unloading cycle. The sheet resistance is measured to be 211  $\Omega/\square$ .

length). Therefore, the strain resolution (1 pixel) is 0.4–0.5%. The substrate stretching was accommodated by the gap increase between CNT\_C and CNT\_D and overlap decrease between CNT\_A and CNT\_B (clearly shown from panel a to c). This observation indicates that the CNTs did not deform as much as the substrate, in other words, sliding occurred between the CNTs and the substrate. Normally upon stretching of the substrate, the CNTs should also be stretched due to the interfacial stress transfer between the substrate and CNTs. Such stress transfer depends on the static friction (interfacial shear

strength) between CNTs and PDMS. Very little is known about the interfacial shear strength between individual nanostructures and PDMS substrates.<sup>[10]</sup> The interfacial shear strength between MWNTs and PDMS is not available in the literature. But the interfacial shear strengths between MWNTs and other polymers have been reported, ranging from tens of MPa to 500 MPa.<sup>[11]</sup> Assuming the interfacial shear strength of 200 MPa between MWNTs and PDMS, the average normal stress in the CNTs is on the order of 100–200 MPa according to the shear-lag analysis,<sup>[12]</sup> which corresponds to an axial strain of 0.05–0.3% in the CNTs depending on how the load is distributed in the shells inside a MWNT (see Supporting Information for more details). Such a small strain corroborates with the negligible CNT elongation under stretching as observed in our optical images. Since the strain in the CNTs was much smaller than the applied strain on the substrate under stretching, CNT/substrate sliding occurred. Upon releasing of the substrate, buckling of all four CNTs was observed (panels d and e). For MWNTs (>4 walls), the critical buckling (normal) stress and strain were estimated to be about 0.44 GPa and 0.044%, respectively.<sup>[13]</sup> Therefore, the average normal stress in the MWNTs as a result of the stress transfer between MWNTs and PDMS should be sufficient to cause CNT buckling before the CNTs slide back to the initial state. Furthermore, the MWNTs might not be completely straight even after the stretching step, which likely leads to a lower buckling stress and strain. This buckle criterion is also in good agreement with our experimental observation. As a reference, the gaps in five panels between CNT\_C and CNT\_D are 9.8, 14.1, 18.2, 17.0 and 14.3  $\mu\text{m}$ , respectively.

Figure 4a shows an atomic force microscopy (AFM) image of a buckled CNT on a PDMS substrate. Clearly the CNT was laterally buckled, on top of the substrate without any noticeable out-of-plane deformation (perpendicular to the PDMS substrate). Note that MWNTs are used in this study. To the best of our knowledge, the present work is the first experimental observation of the lateral buckling of MWNTs (parallel to the PDMS substrate). This lateral buckling mode is different from the previously observed out-of-plane buckling for SWNTs;<sup>[14]</sup> the lateral buckling mode was observed for Si NWs.<sup>[1h,15]</sup> A two-terminal device was fabricated using a buckled CNT on a PDMS substrate to probe how its resistance changes in response to strain. Figure 4b shows a typical *I*–*V* response at a given strain, which clearly exhibited an ohmic contact between the CNT and two electrodes. A sequence of optical images at different strain levels are shown in Figure 4c. The buckled CNT are artificially colored for clarity (see Supporting Information for the original images before colored). The resistance remained nearly constant during a large range of tensile and compressive strains (Figure 4d). Pronounced and modest piezoresistive responses (i.e., resistance change with strain) were reported for straight<sup>[16]</sup> and buckled (wavy)<sup>[14]</sup> SWNTs, respectively. Here for the first time, we found that MWNTs do not exhibit noticeable piezoresistivity when buckled. The maximum bending strain in the MWNT is 4.5% (Figure 4a), which is supposed to cause resistance change of more than two orders of magnitude.<sup>[16a]</sup> However, with the buckled (bending) configuration, the tensile strain on one side of the MWNT is balanced by the compressive strain on the other side; the net strain in the MWNT is the critical buckling strain (~0.044%) or even smaller if the MWNT

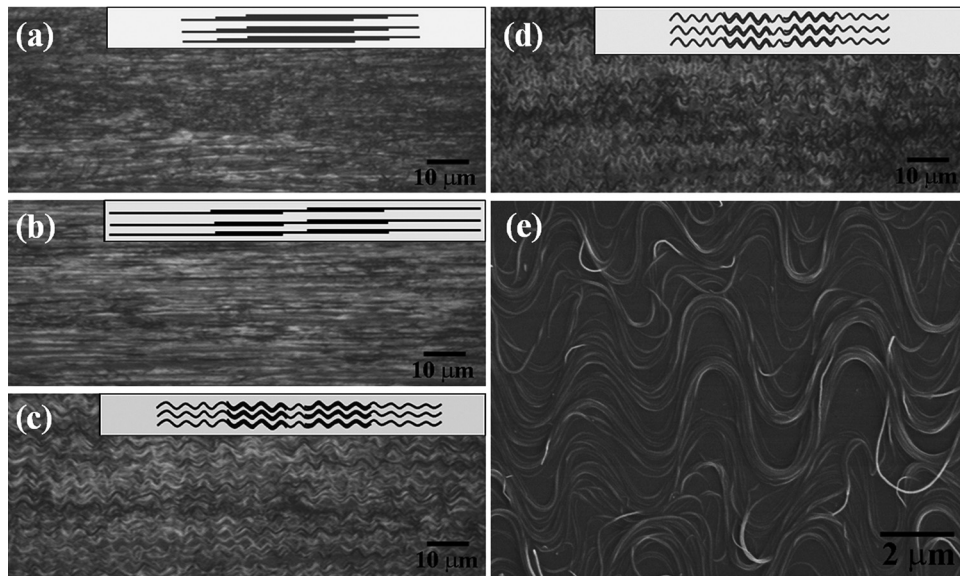


**Figure 2.** (a-d) Optical images of a CNT ribbon on PDMS (a) before stretching, (b) after stretched to 80%, (c) after released to 40% strain, and (d) after released to zero strain. (e) An SEM image of (d) showing the lateral buckling of CNTs.

was not completely straight before buckling. Such a small strain might be responsible for the negligible resistance change. Similar negligible resistance changes were observed for buckled Si nanowires<sup>[1b]</sup> and ribbons.<sup>[17]</sup>

Now we can get back to the electric response of CNT/PDMS conductors under mechanical strain (Figure 1c). When a CNT ribbon is first stretched, intertube sliding (sliding between

CNTs) occurs as a result of the sliding between the CNTs and the PDMS substrate (for example, CNT\_A and CNT\_B in Figure 3a-c). This causes reduction of the overall contact area between the CNTs, thus lead to an increased resistance. Upon the first release of the CNT ribbon, the CNTs buckle and do not slide back (Figure 3d-e). In other words, the contact area between the CNTs in the length direction is about the same as that after stretching (smaller than the initial contact area). This is why the resistance remains nearly constant and does not return to the initial value. The second stretching of the CNT ribbon is essentially the stretching of the buckled CNTs. As shown in Figure 4, the resistance remains constant when a buckled MWNT is stretched, which explains why the CNT ribbon does not show resistance change after second stretching/releasing. Note that the above mechanism is not only applicable to individual CNTs (Figure 3), but also to CNT bundles (i.e., the CNTs might buckle in bundles as shown in Figure 2e).

Our conductors (with CNTs on top of PDMS) are similar to those reported previously (with CNTs embedded in PDMS).<sup>[9]</sup> Our conductors are feasible for meteorology measurements such as SEM and AFM, which directly showed that the interface interaction between the CNTs and the PDMS substrate dictates the buckling of CNTs. In contrast, such meteorology measurements are not feasible for the previous ones. As a consequence, the CNT deformation remains elusive when embedded in PDMS. It is possible that the insights obtained from the present study might shed light on the case of embedded CNTs in PDMS.

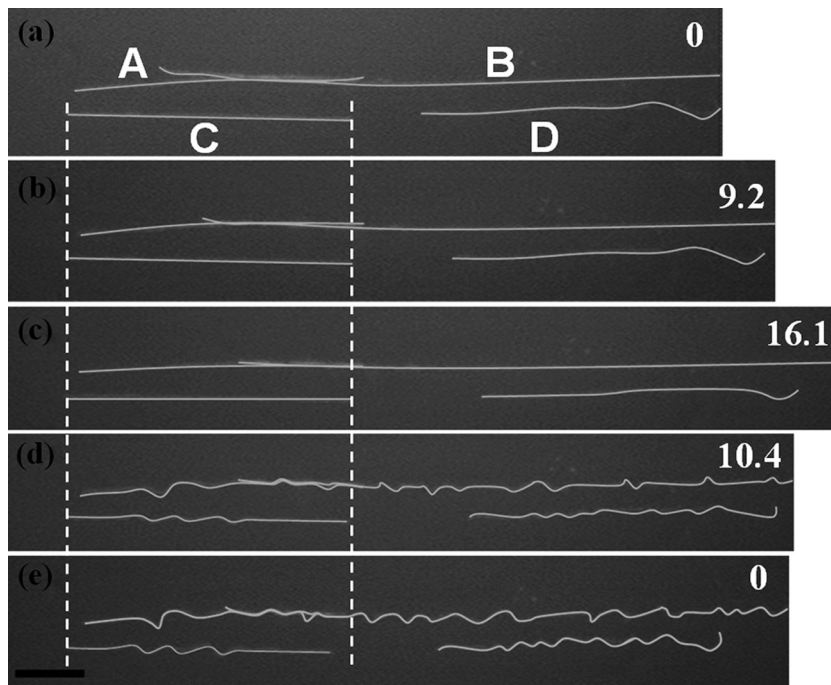


**Figure 3.** Optical images showing the deformation of four CNTs (marked as A, B, C and D) under different strain levels (indicated on the right in percentage) during (a-c) stretching and (d, e) releasing process. Scale bar is 10  $\mu\text{m}$ .



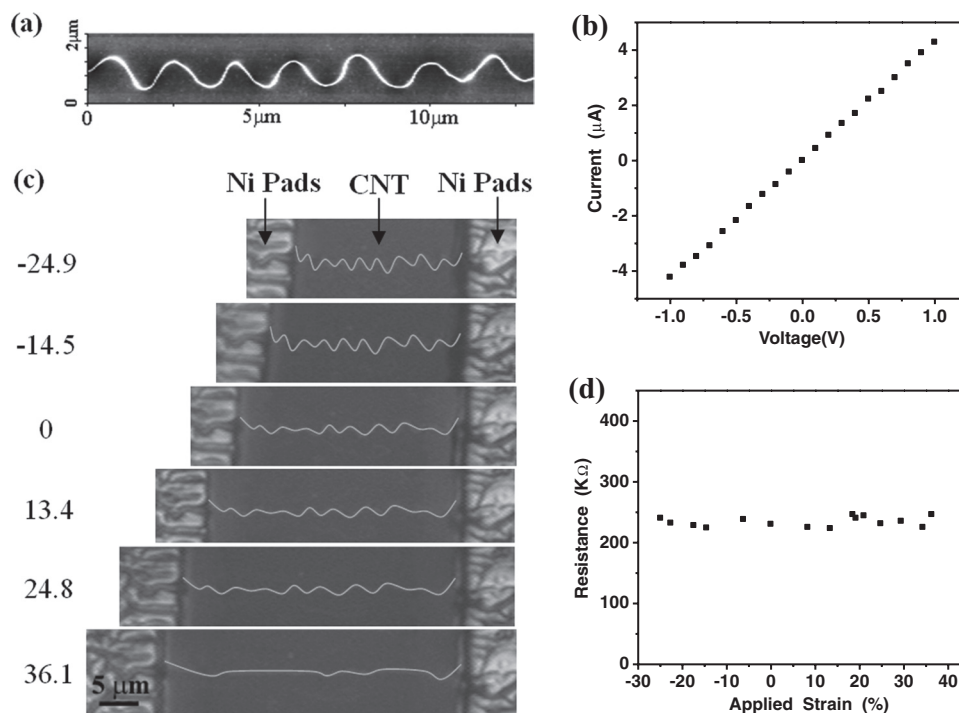


**Figure 4.** (a) AFM image of a buckled CNT on PDMS substrate. (b)  $I$ - $V$  curve of a two-terminal device based on a buckled CNT at 19.2% strain. (c) A sequence of optical images of the buckled CNT device at different strain levels (indicated on the left in percentage). The prestrain for the buckled CNT is 40%. The length of the CNT before buckling is 41.4 μm. (d) The resistance values of the buckled CNT at different compressive and tensile strains.

In conclusion, we systematically investigated the interesting electric response of the aligned CNT ribbons under mechanical strain. We found that CNTs slide on a PDMS substrate under tension, but buckle under compression (releasing). Such an irreversible mechanical deformation is responsible for the observed irreversibility in the electric resistance upon the first stretching/releasing. In addition, we found that the resistance of the buckled MWNTs remains constant under mechanical strain, which explains why the resistance of the CNT ribbon did not change for the second and subsequent stretching/releasing. The CNT ribbon based conductors exhibit superior stretchability (>100%), which may find broad applications in stretchable electronics, sensors, solar cells and touch screens, to name just a few.

Perhaps more significantly, the interface-mediated buckling approach reported here provides an alternative to the well-known prestrain-then-buckling approach<sup>[1a,b]</sup> for fabricating stretchable devices, especially out of aligned nanowires or nanotubes. When combined with tremendous recent progress in nanowire/nanotube alignment and contact printing,<sup>[1g,18]</sup> this new buckling approach could pave the way for large-scale manufacturing (e.g., roll-to-roll process) of nanowire/nanotube based stretchable electronics.

## Experimental Section

**Sample preparation:** Vertically-grown MWNT forests were synthesized using a recently developed chloride mediated chemical vapor deposition (CVD) method.<sup>[19]</sup> With the assistance of a roller, the CNT ribbons were directly drawn from the MWNT forests and attached onto a Teflon substrate, which was wrapped around the roller (See supporting

information). Poly(dimethylsiloxane) (PDMS) substrates with a thickness of 1 mm were prepared using Sylgard 184 (Dow Corning) by mixing the “base” and the “curing agent” with a ratio of 10:1. The mixture was first placed in a vacuum oven to remove air bubbles and then thermally cured at 65 °C for 12 h. Rectangular slabs of suitable sizes were cut from the resultant cured piece. The Teflon substrate with the CNT ribbon was then brought into conformal contact with a PDMS. Because the PDMS has stronger adhesion to CNT than the Teflon substrate, the CNT ribbon was transferred onto the PDMS after the Teflon substrate was slowly peeled. High-purity alcohol was then dropped on the CNT ribbon. The rapid evaporation of the solvent absorbed in the ribbon causes the shrinkage of the film due to the surface tension effects. The adhesion between the CNTs and PDMS are strong enough to hold the buckled structures, which can be reversibly stretched and compressed.

**Electrical characterization:** To measure the resistance of the CNT/PDMS films, silver pastes were applied to the two ends of the CNT ribbon to serve as stretchable electrodes. The CNT/PDMS films were repeatedly stretched and released by a tensile testing stage (Ernest F. Fullam), while the electric resistance was measured at the same time by a multimeter (Agilent, 34401A). It should be noted that the electrode area was left outside of the clamps during the stretching process. To fabricate a two-terminal device based on a buckled CNT on a PDMS substrate, a layer of Ni (400 nm thick) was evaporated through a shadow mask onto the buckled CNT to serve as electrodes. Tensile and compressive strains were applied to the PDMS in the CNT axial direction. The current-voltage ( $I$ - $V$ ) response of the CNT device was measured simultaneously using tungsten probe tips.

## Supporting Information

Supporting Information is available from the Wiley Online Library or from the author.

## Acknowledgements

This work was supported by the National Science Foundation under Award No. CMMI-1030637 (Clark Cooper, program director). We thank Prof. Yuntian Zhu and Xin Wang for providing the CNT ribbons.

Note added in proof: After submitting this paper we learned that an interesting paper with related content had been published.<sup>[20]</sup>

Received: September 2, 2011

Revised: December 4, 2011

Published online: January 23, 2012

- 
- [1] a) J. Song, H. Jiang, Y. Huang, J. A. Rogers, *J. Vac. Sci. Technol. A* **2009**, *27*, 1107; b) J. A. Rogers, T. Someya, Y. G. Huang, *Science* **2010**, *327*, 1603; c) C. Yu, C. Masarapu, J. Rong, B. Wei, H. Jiang, *Adv. Mater.* **2009**, *21*, 4793; d) Z. N. Bao, D. J. Lipomi, B. C. K. Tee, M. Vosgueritchian, *Adv. Mater.* **2011**, *23*, 1771; e) S. P. Lacour, D. Chan, S. Wagner, T. Li, Z. G. Suo, *Appl. Phys. Lett.* **2006**, *88*, 204103; f) T. Sekitani, Y. Noguchi, K. Hata, T. Fukushima, T. Aida, T. Someya, *Science* **2008**, *321*, 1468; g) F. Xu, J. W. Durham, B. J. Wiley, Y. Zhu, *ACS Nano* **2011**, *5*, 1556; h) F. Xu, Y. Zhu, W. Lu, *ACS Nano* **2011**, *5*, 672.
- [2] R. H. Baughman, A. A. Zakhidov, W. A. de Heer, *Science* **2002**, *297*, 787.
- [3] L. B. Hu, W. Yuan, P. Brochu, G. Gruner, Q. B. Pei, *Appl. Phys. Lett.* **2009**, *94*, 161108.
- [4] K. H. Kim, M. Vural, M. F. Islam, *Adv. Mater.* **2011**.
- [5] M. K. Shin, J. Oh, M. Lima, M. E. Kozlov, S. J. Kim, R. H. Baughman, *Adv. Mater.* **2010**, *22*, 2663.
- [6] Y. Y. Huang, E. M. Terentjev, *Adv. Func. Mater.* **2010**, *20*, 4062.
- [7] F. Xu, X. Wang, Y. T. Zhu, Y. Zhu, *Adv. Funct. Mater.* **2012**, DOI: 10.1002/adfm.201102032.
- [8] D. H. Kim, J. L. Xiao, J. Z. Song, Y. G. Huang, J. A. Rogers, *Adv. Mater.* **2010**, *22*, 2108.
- [9] Y. Zhang, C. J. Sheehan, J. Zhai, G. Zou, H. Luo, J. Xiong, Y. T. Zhu, Q. X. Jia, *Adv. Mater.* **2011**, *22*, 3027.
- [10] Q. Qin, Y. Zhu, *ACS Nano* **2011**, *5*, 7404.
- [11] a) H. D. Wagner, O. Lourie, Y. Feldman, R. Tenne, *Appl Phys Lett* **1998**, *72*, 188; b) A. H. Barber, S. R. Cohen, H. D. Wagner, *Appl Phys Lett* **2003**, *82*, 4140; c) Y. Ganesan, C. Peng, Y. Lu, P. E. Loya, P. Moloney, E. Barrera, B. I. Yakobson, J. M. Tour, R. Ballarini, J. Lou, *ACS Appl. Mater. Inter.* **2011**, *3*, 129.
- [12] a) X. L. Gao, K. Li, *Int. J. Solids Struct.* **2005**, *42*, 1649; b) H. L. Cox, *Brit. J. Appl. Phys.* **1952**, *3*, 72.
- [13] J. Xiao, S. Y. Ryu, Y. Huang, K. C. Hwang, U. Paik, J. A. Rogers, *Nanotechnology* **2010**, *21*, 085708.
- [14] D. Y. Khang, J. L. Xiao, C. Kocabas, S. MacLaren, T. Banks, H. Q. Jiang, Y. Y. G. Huang, J. A. Rogers, *Nano Lett.* **2008**, *8*, 124.
- [15] S. Y. Ryu, J. L. Xiao, W. Il Park, K. S. Son, Y. Y. Huang, U. Paik, J. A. Rogers, *Nano Lett.* **2009**, *9*, 3214.
- [16] a) T. W. Tomblor, C. W. Zhou, L. Alexseyev, J. Kong, H. J. Dai, L. Lei, C. S. Jayanthi, M. J. Tang, S. Y. Wu, *Nature* **2000**, *405*, 769; b) E. D. Minot, Y. Yaish, V. Sazonova, J. Y. Park, M. Brink, P. L. McEuen, *Phys. Rev. Lett.* **2003**, *90*, 156401.
- [17] D. Y. Khang, H. Q. Jiang, Y. Huang, J. A. Rogers, *Science* **2006**, *311*, 208.
- [18] a) Z. Y. Fan, J. C. Ho, T. Takahashi, R. Yerushalmi, K. Takei, A. C. Ford, Y. L. Chueh, A. Javey, *Adv. Mater.* **2009**, *21*, 3730; b) C. D. Frisbie, M. J. Ha, Y. Xia, A. A. Green, W. Zhang, M. J. Renn, C. H. Kim, M. C. Hersam, *ACS Nano* **2010**, *4*, 4388; c) T. P. McNicholas, L. Ding, D. Yuan, J. Liu, *Nano Lett.* **2009**, *9*, 3646; d) C. A. Wang, K. M. Ryu, L. G. De Arco, A. Badmaev, J. L. Zhang, X. Lin, Y. C. Che, C. W. Zhou, *Nano Res.* **2010**, *3*, 831.
- [19] a) Y. Inoue, K. Kakihata, Y. Hirono, T. Horie, A. Ishida, H. Mimura, *Appl. Phys. Lett.* **2008**, *92*, 2937082; b) Q. W. Li, X. F. Zhang, R. F. DePaula, L. X. Zheng, Y. H. Zhao, L. Stan, T. G. Holesinger, P. N. Arendt, D. E. Peterson, Y. T. Zhu, *Adv. Mater.* **2006**, *18*, 3160.
- [20] D. J. Lipomi, M. Vosgueritchian, B. C.-K. Tee, S. L. Hellstrom, J. A. Lee, C. H. Fox, Z. Bao, *Nat. Nanotechnol.* **2011**, *6*, 788.
-

## Supporting Information

Original images of Figure 3 before colored

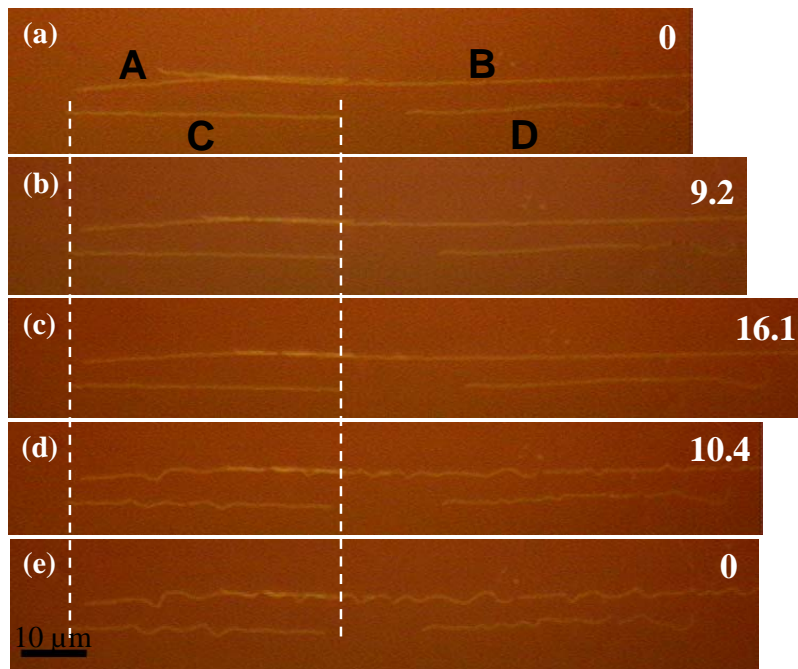


**Figure S1.** Optical images showing the deformation of four CNTs (marked as A, B, C and D) under different strain levels (indicated on the right in percentage) during (a-c) stretching and (d, e) releasing process.

Original images of Figure 4c before colored

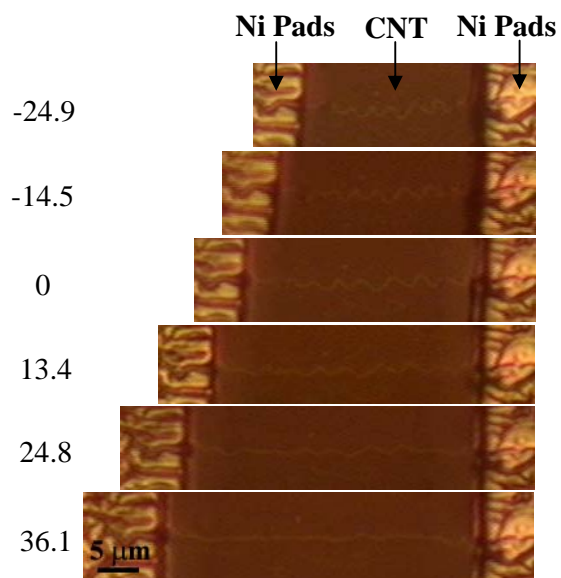


**Figure S2.** Optical images showing the deformation of four CNTs (marked as A, B, C and D) under different strain levels (indicated on the right in percentage) during (a-c) stretching and (d, e) releasing process.

## Shear-lag analysis and CNT buckling

It is important while challenging to analyze the stress transfer between the PDMS substrate and the CNTs. Below we provide a simple analysis, where the CNT/PDMS system is treated as a composite material with PDMS as the matrix and CNTs as the short (discontinuous) fibers. A number of analytical models have been proposed to derive the shear stress distribution and the resulting axial stress in the fiber. One classical approach is the elastic stress transfer model (so-called shear-lag model) developed by Cox in 1952 based on the following assumptions:<sup>[1]</sup> 1) the interface shear stress is proportional to the difference between the displacement of the fiber at a point and the displacement of the matrix at the same point if the fiber were absent; 2) fibers and matrix behave elastically; 3) a perfect bond exists between the fiber and the matrix; 4) no load is transmitted from the fiber ends; 5) stress concentration at the fiber ends is neglected. The normal stress in the fiber and the interfacial shear stress are given by

$$\sigma_f = E_f \varepsilon_m \left[ 1 - \frac{\cosh \beta(l/2 - x)}{\cosh \beta(l/2)} \right] \quad (1)$$

$$\tau_i = \frac{\beta r}{2} E_f \varepsilon_m \frac{\sinh \beta(l/2 - x)}{\cosh \beta(l/2)} \quad (2)$$

where

$$\beta = \left[ \frac{2G_m}{E_f r^2 \log(R/r)} \right]^{1/2}$$

$E_f$  is the fiber modulus,  $\varepsilon_m$  is the matrix strain,  $A_f$  is the cross-sectional area of the fiber,  $G_m$  is the shear modulus of the matrix (= 0.8 MPa),  $l$  is the fiber length (= 40  $\mu\text{m}$ ),  $x$  is the position along the fiber length,  $r$  is the radius of the fiber (= 20 nm), and  $R$  is the interfiber distance. For a single fiber in matrix, a stress transfer parameter  $R/r$  value typically ranges from 2 (a value typical for weak interfaces) to 9 (a value typical for a strong interface).<sup>[2]</sup> Here  $R/r$  value of 5 is used in the analysis.

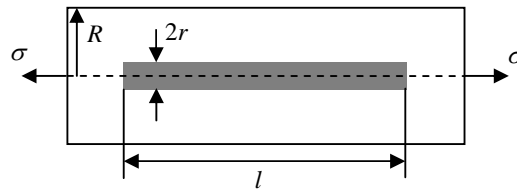


**Figure S3.** Cross-sectional view of a representative volume element considered in the shear-lag model. A short cylindrical fiber (radius  $r$ ) is embedded in a cylindrical matrix (radius  $R$ ).

The fiber in this work is the MWNT. It has been long debated how the mechanical load is distributed between all the shells inside a MWNT. Here we analyze two extreme cases: only the outermost shell takes the load (*i.e.*, hollow fiber) or all the shells take the load equally (*i.e.*, solid fiber). The first case might be pertinent to arc-discharge grown MWNTs with a Young's modulus of 1000 GPa.<sup>[3]</sup> Since the shear-lag analysis is typically for solid fibers, the hollow fiber can be treated as a solid fiber with an equivalent Young's modulus of 34 GPa ( $=E(2t)/R$ , where  $E = 1000$  GPa,  $t = 0.34$  nm, the interlayer spacing between each shell, and  $R = 20$  nm, the average radius of MWNTs used in this work). As an example, when the applied stress on PDMS is 2.4 MPa, the normal stress and interfacial shear stress are plotted in Figure S4(a). It can be seen that the maximum normal stress (or approximately the average normal stress) is about equal to the maximum interfacial stress.

The second case might be pertinent to CVD grown MWNTs that typically possess intershell cross-links, leading to considerable intershell load transfer. The reported Young's modulus for CVD grown MWNTs is 200 GPa.<sup>[2]</sup> Again as an example, when the applied stress on PDMS is 2.4 MPa, the normal stress and interfacial shear stress are plotted in Figure S4(b).



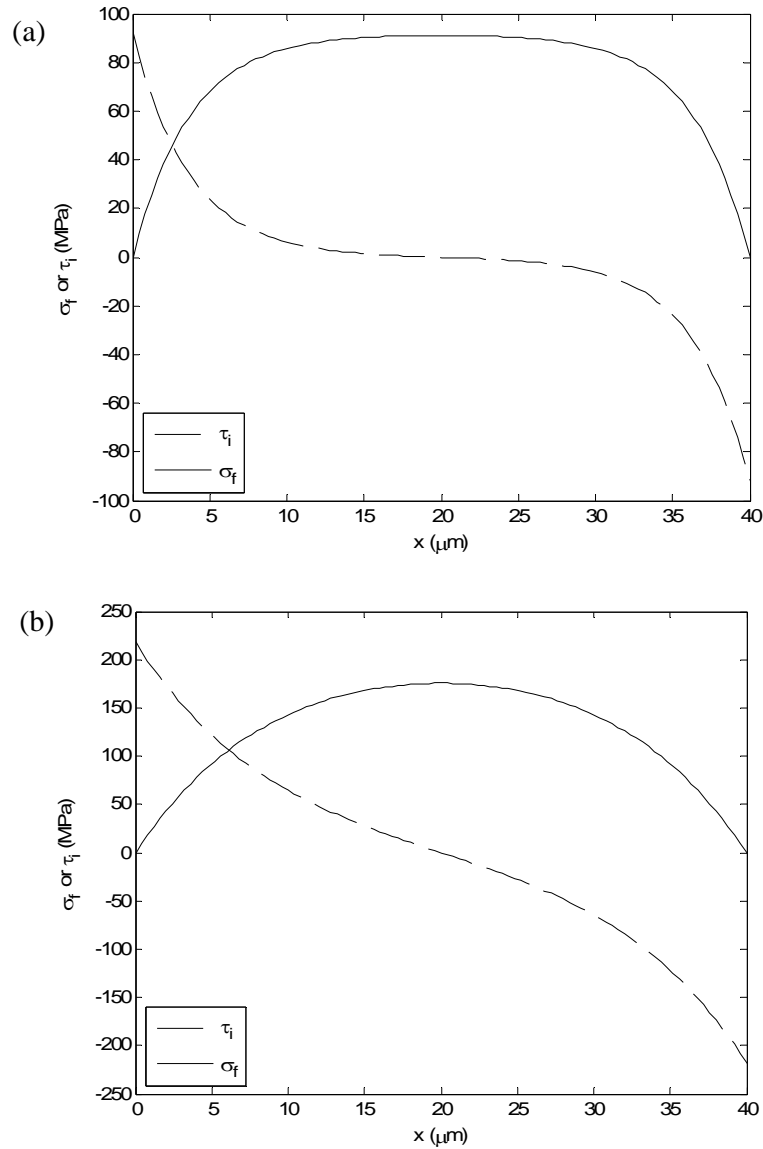


**Figure S4.** The normal stress in a MWNT and the interfacial shear stress at the MWNT/PDMS interface according to the shear-lag analysis. (a) The first case where the outermost shell takes the load (note that in this plot the normal stress is on the equivalent solid fiber). (b) The second case where all the shells take the stress equally.

The interfacial shear strength between MWNTs and PDMS is not available in the literature. But the interfacial shear strengths between MWNTs and other polymers have been reported, ranging from tens of MPa to 500 MPa.<sup>[4]</sup> In both cases discussed above, suppose the interfacial shear strength is 200 MPa, the average normal stress in the MWNTs can be easily larger than 100 MPa. In the first case, 100 MPa normal stress in the equivalent solid fiber

corresponds to  $\sim 3$  GPa stress in the outermost shell, which leads to 0.3% axial strain. In the second case, 100 MPa normal stress corresponds to 0.05% axial strain. Under tension, such small strains in both cases are beyond the strain resolution of our optical microscope. However, under compression, it is a totally different scenario. Xiao et al. predicted that the critical buckling strain for MWNTs under compression is 0.044% (for number of shells larger than 4).<sup>[5]</sup> Therefore, such small axial strains (in both cases) in the MWNTs are sufficient to cause their buckling. The above simple analysis agrees very well with our experimental observation under both tension and compression. It should be noted that since our MWNTs are CVD grown, the second case might be more relevant to this work.

Also note that our system is a fiber on a substrate (should be partly embedded in the substrate). It has been assumed that the contact width is equal to the CNT diameter (*i.e.*, half of the CNT is embedded in the substrate).<sup>[5]</sup> Our analysis of a fiber totally embedded in a matrix might overestimate the normal stress in the fiber by a factor of two. To thoroughly understand the stress transfer between CNTs and the PDMS substrate, several further studies are warranted including: 1) measurement of the Young's modulus of our MWNTs (which might be process dependent) and understanding of the exact stress distribution inside the MWNTs; 2) measurement of the interfacial shear strength between MWNTs and PDMS; 3) a more rigorous shear-lag analysis and likely finite element analysis of our system.

**Experimental setup for drawing CNT ribbons**

Figure S5 is an optical image showing the experimental setup used in the drawing process. With the assistance of a roller, the CNT ribbons were drawn and attached onto a Teflon substrate, which was wrapped around the roller.

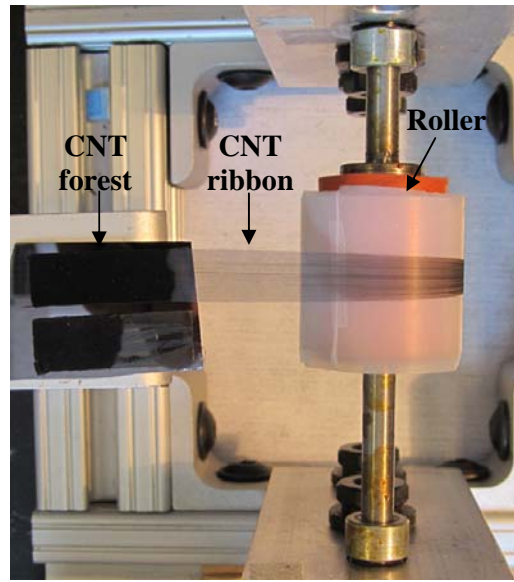


**Figure S5.** Optical photograph of the assembly apparatus used in our experiments to draw the CNT ribbon and attach it onto the Teflon substrate.

## References

- [1] a) H. L. Cox, *Brit. J. Appl. Phys.* **1952**, 3, 72; b) J. A. Nairn, *Mech. Mater.* **1997**, 26, 63.
- [2] Y. Ganesan, C. Peng, Y. Lu, P. E. Loya, P. Moloney, E. Barrera, B. I. Yakobson, J. M. Tour, R. Ballarini, J. Lou, *ACS Appl. Mater. Inter.* **2011**, 3, 129.
- [3] M. F. Yu, O. Lourie, M. J. Dyer, K. Moloni, T. F. Kelly, R. S. Ruoff, *Science* **2000**, 287, 637.
- [4] a) H. D. Wagner, O. Lourie, Y. Feldman, R. Tenne, *Appl. Phys. Lett.* **1998**, 72, 188; b) A. H. Barber, S. R. Cohen, H. D. Wagner, *Appl. Phys. Lett.* **2003**, 82, 4140; c) A. H. Barber, S. R. Cohen, A. Eitan, L. S. Schadler, H. D. Wagner, *Adv. Mater.* **2006**, 18, 83.
- [5] J. Xiao, S. Y. Ryu, Y. Huang, K. C. Hwang, U. Paik, J. A. Rogers, *Nanotechnology* **2010**, 21, 085708.